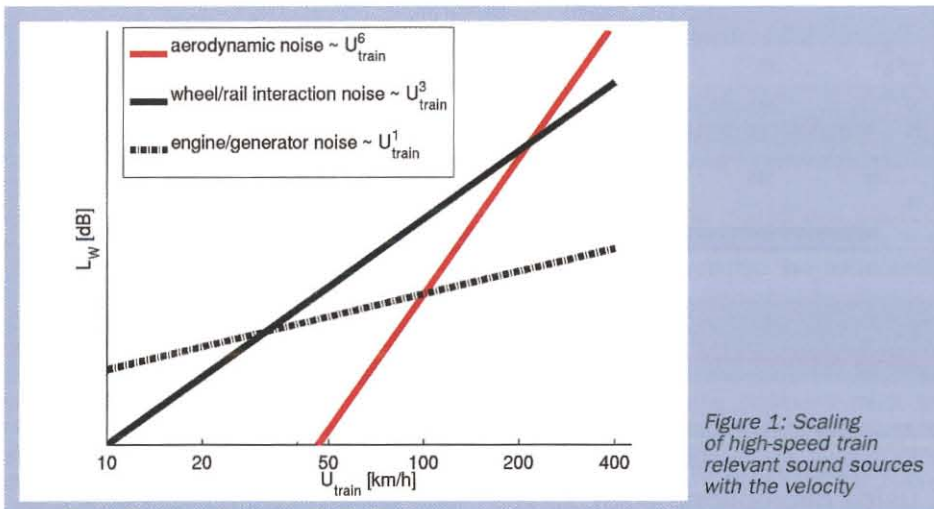


Activities in acoustics

Approaching high-speed railway vehicle acoustics as a corporate multi-domain task. Increasing the attractiveness and society's acceptance of rail transport is defined as an important aspect within the overarching aims of the Next Generation Train (NGT). Due to their impact on passengers and residents, external noise emissions and internal structure-borne and airborne sound transmission, are fundamentally undesirable properties of rail vehicles. An ambitious project such as the NGT must thus place increased emphasis on the avoidance and reduction of noise and vibrations. Furthermore, from an economic perspective it appears attractive to counter acoustic issues as close to the source as possible and not to rely on infrastructural noise reduction measures [1].



Noise emission from rail vehicles is a heterogeneous problem, as a large number of individual sources, such as aeroacoustics, rolling noise, motor, brakes, etc., can be identified [2]. Acoustic considerations were therefore taken into account in decisions as early as the creation of the NGT vehicle concept. The aeroacoustic disadvantages of pantographs thus formed one of many arguments favouring an alternative, contact-free system of energy transmission (cf. RTR Special – NGT: The NGT propulsion concept). When creating the running gear a design was chosen that is in particular capable of steering the wheel pair in curve motion [cf. RTR Special – NGT: Running dynamics concept with mechatronic guidance] in order to minimise the risk of curve squeal, primarily relevant in residential areas near stations.

However, this vehicle concept also creates conflicts of interest, i.e. mainly due to the fact that the NGT is a high-speed train. As an illustration, Figure 1 shows the influence of different speed-dependent noise factors. The aeroacoustically induced noise sources increase with approximately the sixth power of train velocity. The optimisation of aeroacoustic characteristics is therefore an important factor during the development of the NGT.

Consequently, this article begins with a representation of different aeroacoustic experiments on high-speed trains both outdoors and in wind tunnels as well as the development of measurement technology necessary to this end. This is followed by an example of the design of active systems to reduce the transmission of internal aeroacoustically induced noise. The final part introduces a calculation model for early consideration of acoustic aspects during the development of the running gears.



Dipl.-Phys.
Sigfried Loose

Scientist

DLR-Institute of Aerodynamics and Flow Technology, Fluid Systems, Göttingen
Sigfried.Loose@dlr.de



Dipl.-Phys.
Andreas Lauterbach

Scientist

DLR-Institute of Aerodynamics and Flow Technology, Fluid Systems, Göttingen
Andreas.Lauterbach@dlr.de



Dr.-Ing.
Stephan Algermissen

Scientist

DLR-Institute of Composite Structures and Adaptive Systems, Adaptive Systems, Braunschweig
Stephan.Algermissen@dlr.de



Dr.-Ing.
Andreas Heckmann

Scientist

DLR-Institute of Robotics and Mechatronics, Systems Dynamics and Control, Oberpfaffenhofen
Andreas.Heckmann@dlr.de

1 Development of a Line Array for Drive-by test of trains

In the first step of the investigations, a line array comprising 20 microphones was developed to separate aeroacoustically induced noise, which is created by airflow around the vehicle, and wheel/rail interaction noise, which is created by the interaction of the bogies and the track. This array was implemented during a measurement campaign on a Spanish high-speed train. The measurements also provide an important foundation for testing routines developed on the basis of the delay and sum beamforming algorithm with real data.

This design with a horizontal array allows source separation in a horizontal direction. Figure 2 shows a photo of the design and Figure 3 gives an overview of the local strength of the sound sources that appear on the Talgo 350 at a speed of 200 km/h. The sound pressure level is colour-coded in dB. The study has shown that at high-speed, frequencies from 5 kHz are dominated by aerodynamic noise sources.

In order to increase the spatial resolution along the train a new type of microphone array was developed. This comprises a line array in combination with a two-dimensional elliptic acoustic mirror [3]. This design was successfully tested on a high-speed train track in Germany (see Figure 4), which is used by different types of Inter City Express (ICE) and other passenger trains.

It was possible to improve the quality of the results. The source separation works successful using the properties of the elliptic mirror along the x-axis and in the beamforming methods along the y-axis. The combination of both techniques allows a three-dimensional reconstruction of the source distribution. Individual wheel sets and aeroacoustic noise in the roof area caused by roof structures can be localised in the source maps (Figure 5).



Figure 2: The Talgo 350 passes the line microphone array.

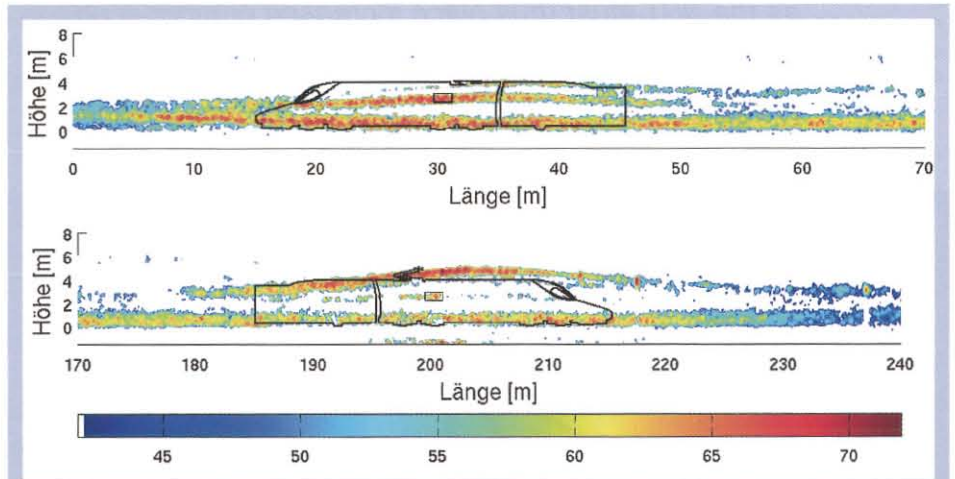


Figure 3: Talgo 350 source map. The sound pressure level is colour-coded in dB. The highest levels are in red.

2 Aeroacoustic wind tunnel investigations on train models using microphone array measurement technology

In the past, numerous aeroacoustic investigations have been conducted on aeroplanes

and their components. These provide knowledge concerning noise source, source volume and possibly the source mechanism. The results represent the basis for noise prediction software tools. Acoustic measurement technology familiar from aeronautics was used to develop a quiet NGT.



Figure 4: Test configuration on the track and laboratory configuration with an array comprising a line array and an elliptic acoustic mirror

Relatively weak noise sources can generally be expected on a train, which means higher requirements for the measurement technology.

The investigations began with a microphone array of 48 microphones and an aperture of 1 x 2 metres. However, the first measurements in the 1-metre wind tunnel demonstrated that the combination of the small number of microphones and the loud wind tunnel made it almost impossible to clearly localise the train's noise sources. A larger number of microphones is necessary in order to increase the signal to noise ratio and expand the spectral bandwidth. It is a characteristic of microphone arrays that the response to a monopole point source is convoluted with a so-called point spread function (PSF); in addition to a main maximum, a number of side lobes appear in the evaluation plane. Figure 6 provides an example of how the array response can look on a monopole source. The main to side lobe relation determines the maximum dynamic that can be achieved with the microphone array. The quieter the sources of the train model in comparison to disturbing background noise are, the larger the dynamic range of the array must be. Otherwise the source is indistinguishable from the background noise. The shape of the PSF depends on the frequency and on the microphone layout. A layout optimisation routine was developed in order to improve the dynamic over a wide frequency range. A monopole source in front of the array was simulated. A Gauss distribution was used as the target function. A minimum of deviation between the simulated PSF and the Gauss distribution can be iteratively determined by successively adjusting each individual microphone position. After a sufficient number of iteration steps one achieves a microphone layout with an optimised dynamic range.

In the course of further developments the array was expanded to 143 microphones. Figure 7 shows the microphone array with the optimised three-dimensional microphone layout in the measurement section of the aeroacoustic wind tunnel. The train model can be recognised in the foreground of the measurement section. It is mounted on a ground board, which is designed to peel the boundary layer of the wind tunnel. This experiment is described in detail in [4]. With this design, the sound passes along the wind tunnel shear layer from the source to the array microphones. Within the flow, the sound is convected and finally refracted on the shear layer. This leads to phase and amplitude distortions, which must be taken into account using suitable corrections to the shear layer, as otherwise the position and volume of the source cannot be determined correctly. There is also a loss of quality in the measurement results [5]. A correction according to Amiet [6], which takes the influence of the shear layer into account, was included in the evaluation routine.

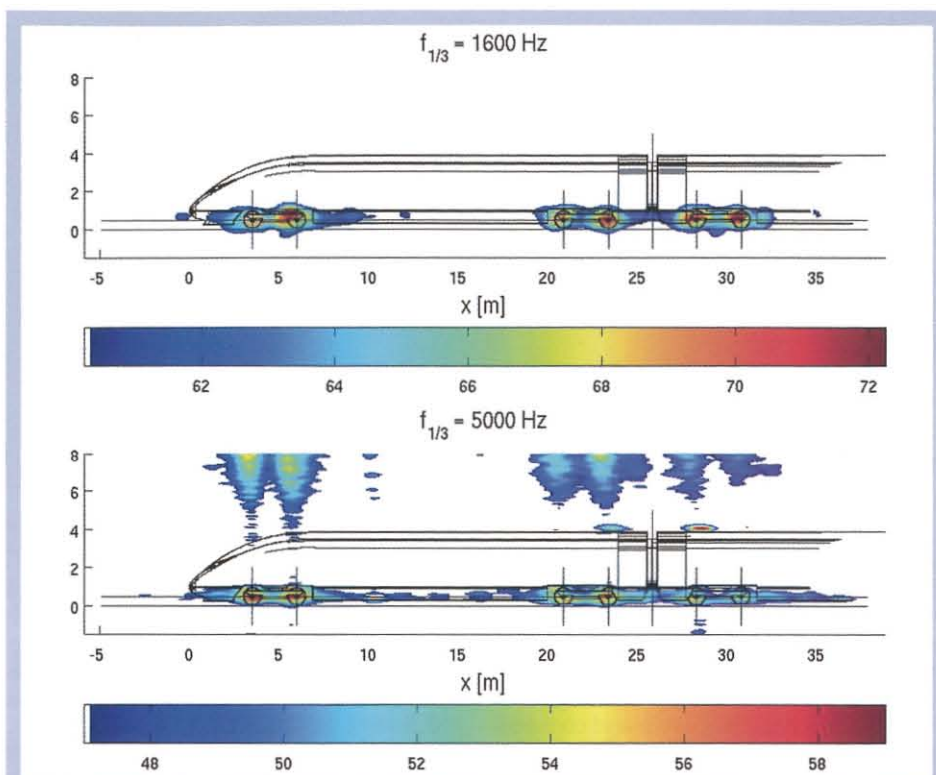


Figure 5: ICE 3 source maps for two selected third-octave bands at a speed of $U = 200$ km/h. The sound pressure level is colour-coded in dB.

The precision of the microphone positioning emerged as another criterion affecting the quality of the results. The more accurate the individual microphones positions are known to be, the higher the maximum achievable dynamics. The higher the observed frequencies, the more accurate the individual microphone positions must be known to be; otherwise there will be inaccuracies between the phase relationships of the microphone signals. As the measurements are conducted on scaled-down models (in the present investigation models on a scale of 1:25 were used) it can be assumed that the observed frequency range will move to higher frequencies. As-

suming a linear scaling of frequencies with the scale of the model, then frequencies far into the inaudible range of up to 50 kHz can be expected. This frequency range requires a positional accuracy in the range of a few 1/10 mm, which, for example, is practically impossible to measure using a measuring tape. Therefore a process of calibration was developed that can determine the position of microphones within the necessary range of accuracy [7 and 8]. In principle, this process functions in a very similar way to the Global Positioning System (GPS); in this process, optical path differences to several satellites are used to triangulate the position. For the case of

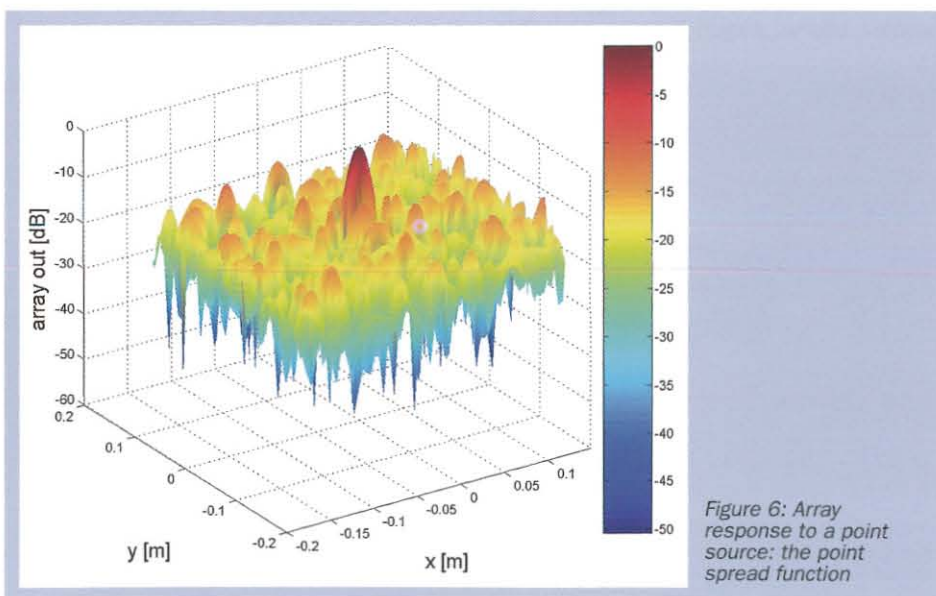


Figure 6: Array response to a point source: the point spread function



Figure 7: Train model mounted on a ground board in the AWB measurement section, Braunschweig. In the background is the microphone array, positioned out of the flow.

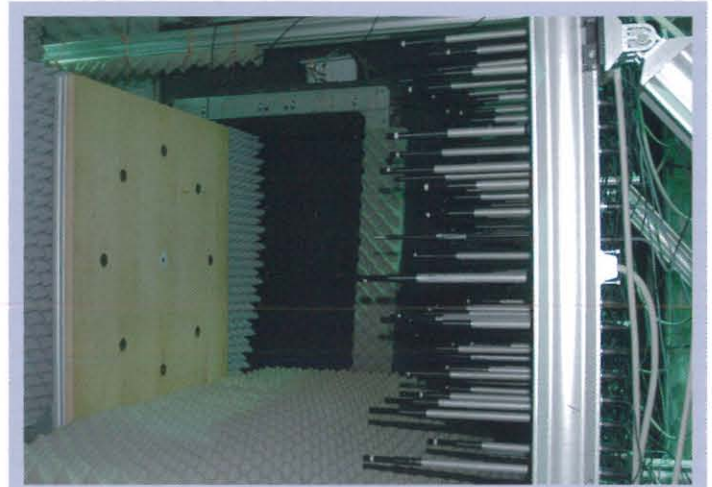


Figure 8: Phase calibration of the microphone array: on the left is the board with the 8 noise sources and the reference microphone; on the right are the array microphones.

phase calibration, a calibration device was developed consisting of a board in which 8 unipolar-like noise sources are integrated. These are arranged in a circle and consecutively emit white noise. There is also a reference microphone in the centre of the circle. Using correlation analysis, the 8 distances between the sources and the selected ar-

ray microphone can be determined. The position of the array microphone can be calculated to a high level of accuracy ($\delta x < 0.5$ mm) using a triangulation algorithm. Figure 8 shows the calibration device in practical use in the measurement section within the aeroacoustic wind tunnel. The measurements on an ICE 3 model with a

scale of 1:25 provide insights into trains' noise sources.

Figure 6, above, shows the source map for a flow velocity of $U_\infty = 40$ m/s. The source strength is colour-coded in dB. It illustrates that spatial resolution must be improved at low frequencies in particular. Furthermore, in the test configuration used, acoustic reflections occur that appear in the form of mirror sources in the source maps. A so-called deconvolution algorithm was therefore used, which detects coherent contributions in the source maps and removes them from the result (CLEAN_SC [9]); the result is illustrated in Figure 6 below. Coherent contributions in source maps can be either side lobes of the PSF or physical reflections, such as occur on the ground board. As well as being localised, noise sources can also be quantitatively investigated in detail in the form of spectra calculated via spatial integration over predefined areas. The areas concerned are those of the first bogie and the pantograph. The areas are indicated by the boxes in Figure 10 above. The spectra illustrate completely different dependencies on the flow velocity, and the two source mechanisms are fundamentally different.

The wind tunnel experiments conducted to this point provide insights into sound sources on an ICE 3 model with Reynolds numbers of up to $Re = 0.5 \times 10^6$ (based on the width of the train). An actual travelling train reaches Reynolds numbers of up to $Re = 16 \times 10^6$. As an extrapolation of the results from the aeroacoustic wind tunnel would be questionable at these high Reynolds numbers, wind tunnel investigations on the same model at higher Reynolds numbers are necessary. An increase can, for example, be achieved by cooling the fluid, as this reduces the kinematic viscosity.

By cooling it to temperatures as low as 100 K and a maximum Mach number of $Ma = 0.3$, Reynolds numbers of up to $Re = 3.7$ million can be achieved. Figure 11

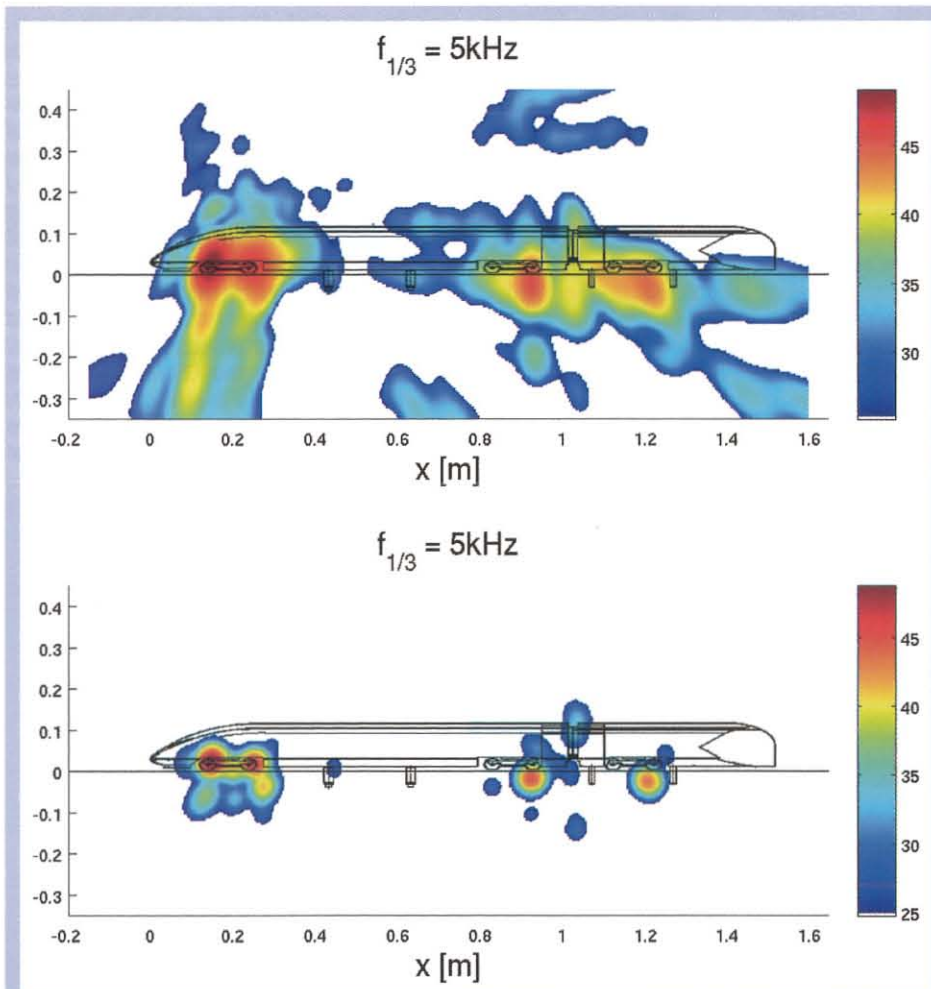


Figure 9: ICE source maps at $U_\infty=40$ m/s. Above, results given by standard beamforming. Below, the result of the same measurement using CLEAN_SC

shows the operational range for the German-Dutch Wind Tunnel's (DNW) cryogenic wind tunnel (DNW-KKK) at the German Aerospace Center (DLR) in Cologne. It was here that the following measurements were conducted. A microphone array suitable for these low temperatures was developed for this purpose [10]. Figure 12 illustrates the experimental design.

There are some differences between the measurements in the DNW-KKK and those at the Aeroacoustic Wind Tunnel Braunschweig (AWB). The cryogenic wind tunnel is not optimised for aeroacoustic investigations. The closed measurement section comprises soundreflecting walls, which can cause acoustic reflections. In addition, oscillation eigenmodes can form in the wind tunnel tubes, which can seriously affect the results. Here too, a ground board was used to peel the tunnel boundary layer. This board sits on a number of bolts; no part of the construction is aeroacoustically optimised and the resulting noise affects the array measurements. All this leads to results with a comparatively low signal/noise ratio. The focus of the experiments was placed on the aeroacoustically induced noise of the first bogie. In addition, the planned high NGT speeds as double-decker train sets are already encroaching upon areas where measures for securing safe driving dynamics are necessary. The use of a front spoiler and its influence on both the aerodynamics and aeroacoustics were therefore tested. Figure 13 shows the modification at the head of the ICE 3. The ICE 3 serves as the primary test rig, as the aerodynamic coefficients for this model are already known from a large number of investigations.

For further investigations, considerations were put forward to enhance the otherwise typical setup with the model mounted on a ground board in order to improve simulation of the flow conditions in the wind tunnel. The noise sources investigated are influenced by the flow near ground level. Depending on the aerodynamic length, the boundary layers that occur on the ground board in the laboratory

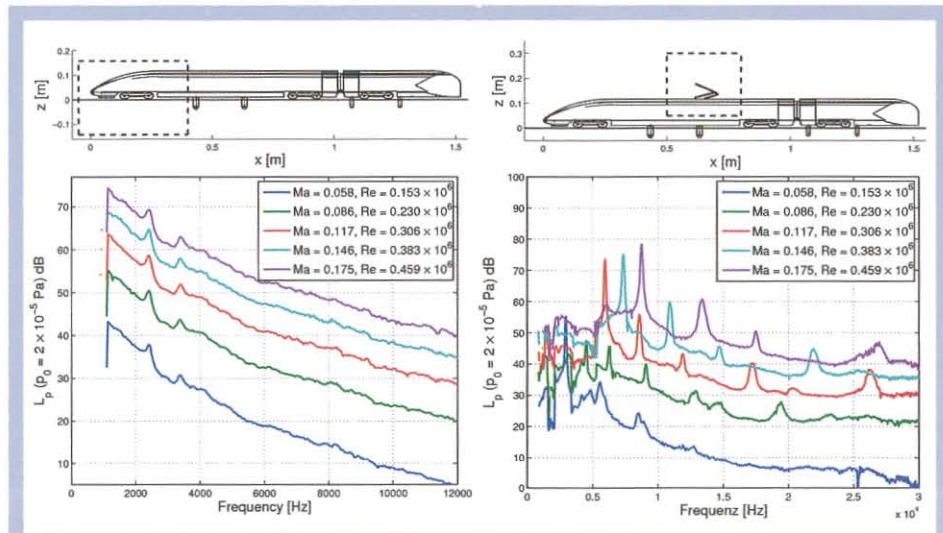


Figure 10: Focused spectra above the area of the first bogie (left) and above the area of the pantograph (right) for different flow velocities

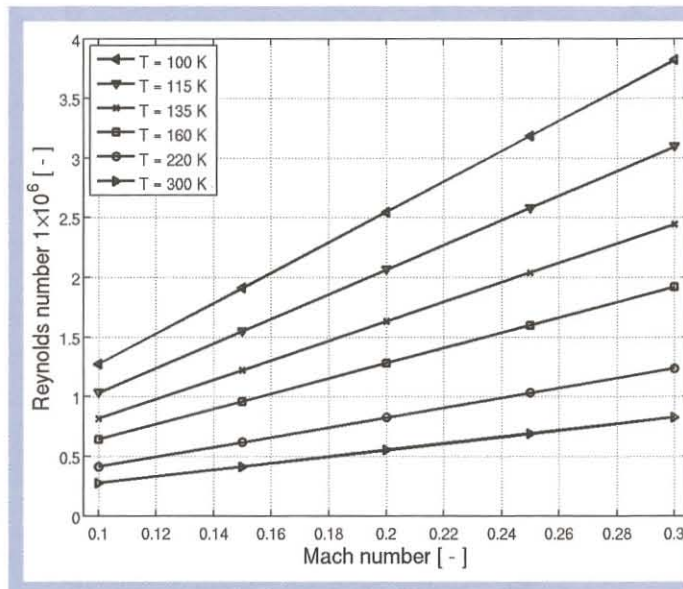


Figure 11: The operational range of the DNW-KKK

experiment merge with the boundary layer underneath the train set to form a Poiseuille-like flow. With a travelling train set, on the other hand, a turbulent Couette flow, which

has a different boundary layer profile, can be observed between the underside of the train and the ground. The second version of the NGT has covered bogies, whose influence



Figure 12: Setup inside the DNW-KKK test section: The train model is installed on a rotating ground board; the microphone array is installed on the wind tunnel wall.



Figure 13: The ICE3 model equipped with a front spoiler; its influence on both the aerodynamics and aeroacoustics were tested.



Figure 14: The setup of the double model inside the DNW-KKK test section; the microphone array is installed on the wind tunnel wall.

on the aerodynamics and aeroacoustics was investigated. For this investigation particular attention should be paid to the best possible simulation of flow near ground level. For this reason a double model configuration was chosen. Figure 14 shows the design in the measurement section of the cryogenic wind tunnel. The plane of symmetry between the two models represents the ground and, therefore, there is no undesired boundary layer on the ground. This entire design also has a positive effect on the results of the aeroacoustic investigations, as there can be no acoustic reflection on the ground board and there is no background noise caused by the ground board and its mounting.

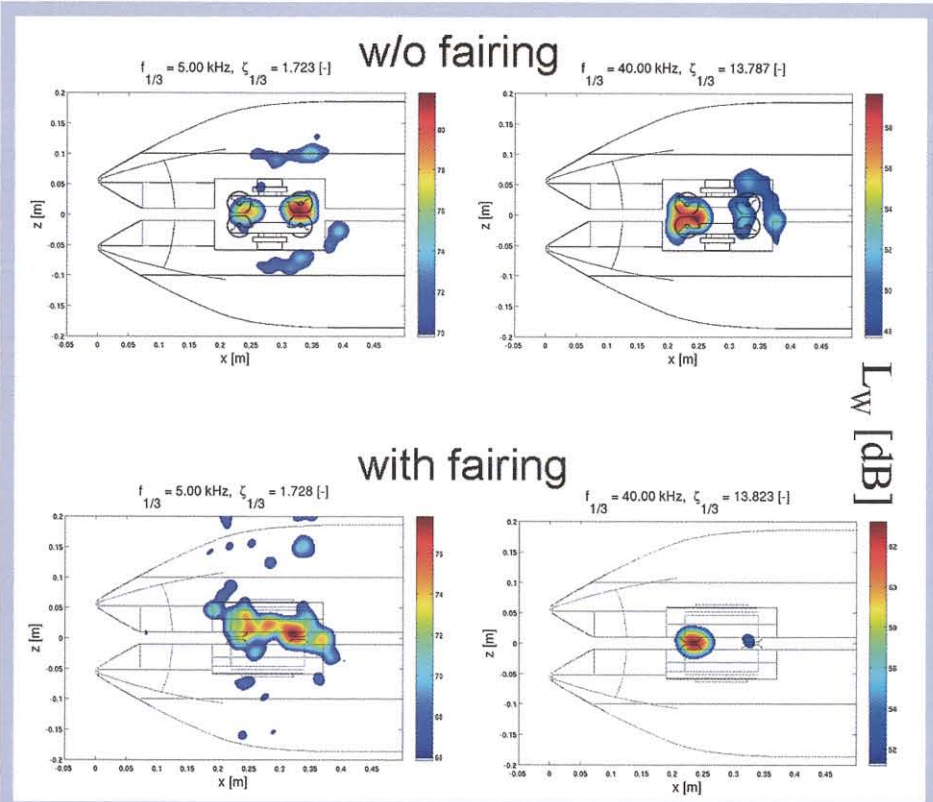


Figure 15: Source maps for two different 1/3 octave bands of the configurations with and without bogie fairings. The sound power level is colour-coded in dB.

Figure 15 shows source maps for the front area of the double model. The inflow velocity is $Ma = 0.3$ and the Reynolds number $Re = 0.85 \times 10^6$ (measured at the room temperature of $T = 290$ Kelvin). Noise sources in the bogie area can be clearly localised. Integrated spectra for measurements at low Reynolds numbers ($Re = 0.85 \cdot 10^6$) and high Reynolds numbers ($Re = 3.72 \cdot 10^6$) for configurations with and without fairing are illustrated in Figure 16. The fairing leads to a broad reduction in noise of 2–3 dB, which is particularly pronounced at high Reynolds numbers. At low Reynolds numbers there are tonal components in the spectra for the configuration with fairing. It is suspected that the closed configuration tends to excite the cavity modes. This excitation is dependent on Reynolds numbers and occurs more prominently at lower Reynolds numbers. If this tendency is followed, it can be assumed that these disruptive tonal components are almost impossible to excite on a real train. More details can be found in [11].

3 Robust control of Turbulent Boundary Layer (TBL) Noise

Introduction

Constantly increasing driving speeds also increase the influence of aerodynamically induced noise on the internal noise level of

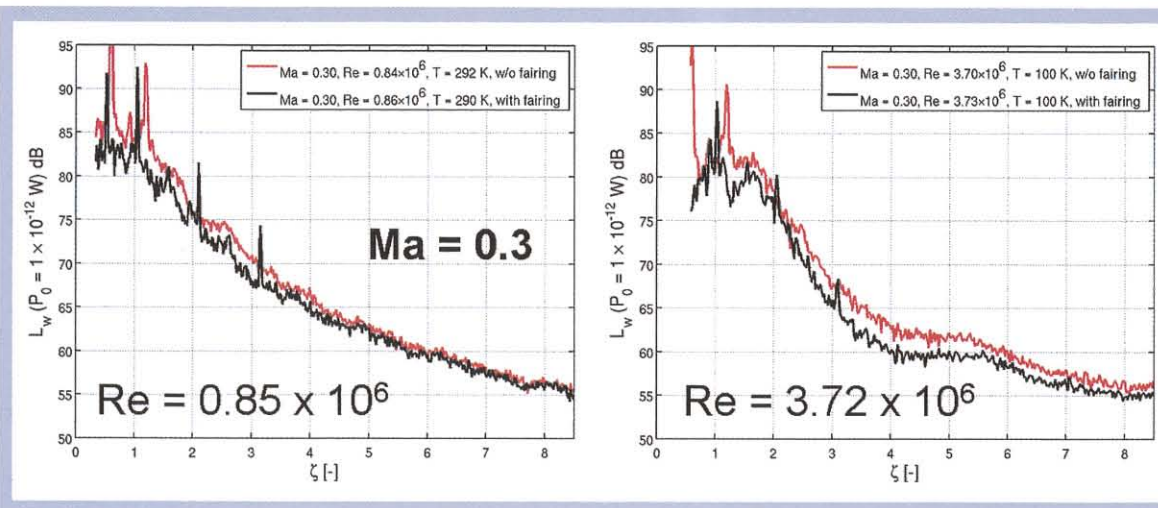


Figure 16: Integrated spectra. Comparison of the setup with and without mounted bogie fairings, at two different Reynolds numbers at constant Mach number $Ma = 0.3$

the train set. The source of this noise is the turbulent boundary layer (TBL) caused by air flowing around the structure of the train. Its vortex structures, which are strongly uncorrelated spatially and with regard to time, create a broadband, stochastic excitation of the structure on the outer surface of the train set. This excitation is conducted to the inner walls of the train set as structure-borne noise and finally conducted to the passengers as emitted airborne sound. Consequently, the acoustic comfort of the passengers is dependent upon the drastic increase in noise generation via aerodynamic effects at high speeds. In order to guarantee the standard of comfort of modern high-speed trains for those of the future, new processes for avoiding or halting sound immissions into the train set must be found.

The German Aerospace Center (DLR) has long conducted research into active systems to reduce structural noise transmission. The use of so-called Active Structural Acoustic Control (ASAC) can reduce or change the noise emission of a structure. Sensors on the structure measure vibration in a normal direction, which is regulated by a control algorithm. Using a model that describes the vibration behaviour and the noise emission of the structure, the controller is able to calculate suitable control signals for the actuators on the structure. The following section introduces experiments at the German Aerospace Center (DLR) in Braunschweig, which tested such an active system on a carbon fibre reinforced plastic (CFRP) panel under influence of flow.

Experimental setup

The aeroacoustic wind tunnel of DLR in Braunschweig has an open test section. The nozzle has a cross-section of $1.2 \times 0.8 \text{ m}^2$ and the maximum wind speed is 60 m/s or Mach 0.17. The test section is enclosed by an anechoic chamber to enable acoustic measurements. For realization of TBL experiments, a closed test section has been de-

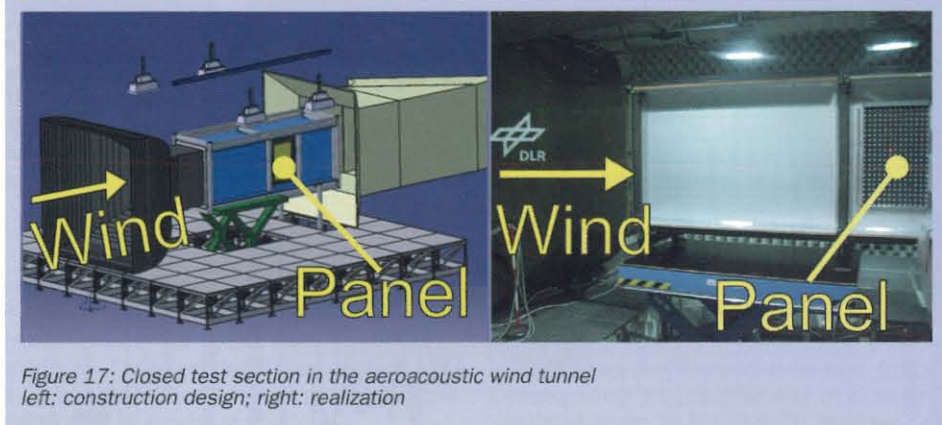


Figure 17: Closed test section in the aeroacoustic wind tunnel left: construction design; right: realization

signed and built. In Figure 17 the construction design and a picture of the realization can be seen. The test section is a rectangular channel that is placed right behind the nozzle. For vibration decoupling, the test section is mounted on shock absorbers. The carbon fiber reinforced plastics – CFRP panel is placed in a side wall of the test section. The thickness of the TBL is steadily growing in the closed test section to app. 41 mm at Mach 0.17 until it reaches the panel.

The panel is made of CFRP and has a clearance of $500 \times 800 \text{ mm}^2$. Figure 18 shows the panel after the fabrication process without actuators and sensors. The four L-stringers and the aluminum frame for fast mounting are bonded to the panel. When mounted in the test section, the stringer side will radiate sound into the anechoic chamber.

For control actuating and sensing the panel is equipped with five DuraAct® P-876.A15 piezo patch actuators (Dim: $61 \times 35 \times 0.8 \text{ mm}^3$) and ten PCB® 352A24 accelerometers. The actuators were bonded in vacuum to ensure excellent strain transmission. Actuator's maximum voltage is 1000 V . The actuator positions were calculated with an in-house ASAC pre-design tool in order to achieve maximum noise reduction [14]. The sensor positions are chosen for good observability of all eigen-

frequencies in the control bandwidth. The final active panel mounted in the closed test section is shown in Figure 19.

Control

For good control performance an accurate description of the controlled plant G , from actuators to sensors, must be available. Due to inaccurate parameters, models from finite element calculations lack precise description of vibration behavior; especially phase response is characterized poorly. Therefore, models for control synthesis are generated by experimental system identification using experimental data. Here, multi-reference excitation is applied for system identification: The five piezo patch actuators excite the panel structure with uncorrelated random noise simultaneously and accelerometers record the structural responses. From these 15 time signals a subspace based identification algorithm [15] generates a discrete state-space model of the controlled plant. A maximum number of 90 states ensures a good accuracy of the model.



Figure 18: Passive CFRP panel after fabrication

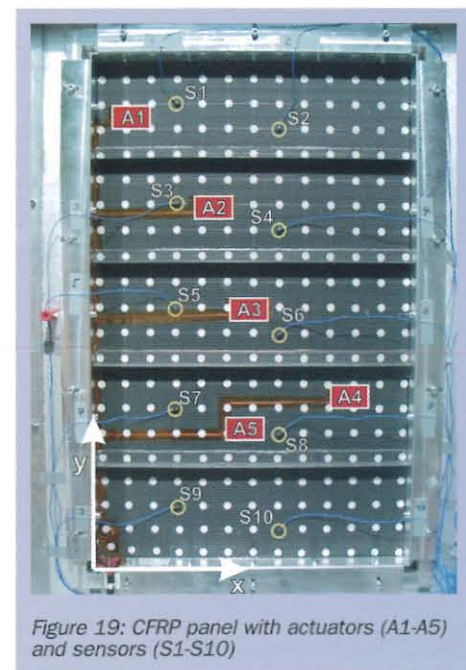


Figure 19: CFRP panel with actuators (A1-A5) and sensors (S1-S10)

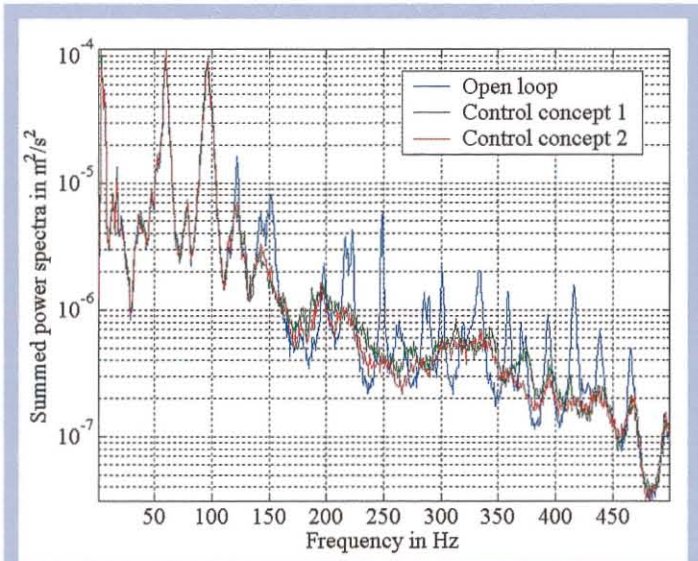


Figure 20: Vibration reduction (local control = concept 1, global control = concept 2)

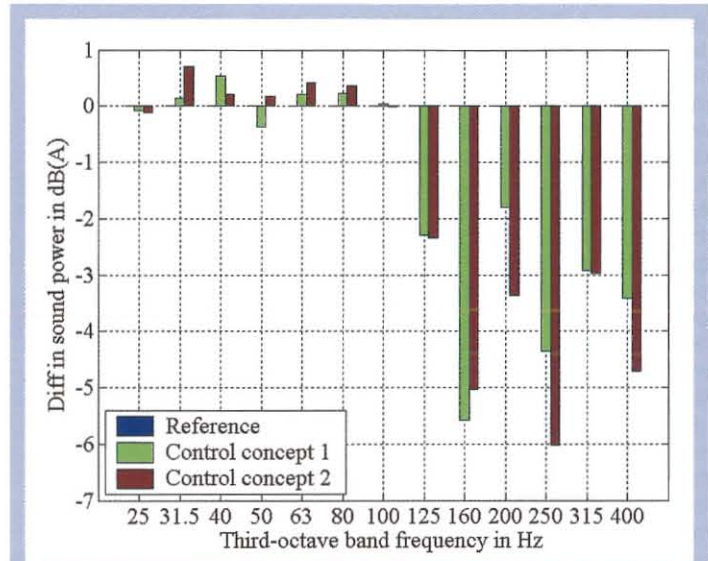


Figure 21: Radiated sound power reduction (local control = concept 1, global control = concept 2)

The bandwidth of the system identification and control is set to 500 Hz. The first eigenfrequency of the controlled plant is located at 122 Hz. Therefore, control authority below 122 Hz is not available. For generating a robust controller the so-called H_{∞} control algorithm [13] is used.

Experiments

Several control concepts were implemented and tested in experiments in the closed test section of the aeroacoustic wind tunnel from which two are presented in this article: A local and a global concept. The local concept aims to reduce the vibrations at the sensor locations whereas the global concept achieves it on a “virtual” sensor grid. This grid consists of 13 x 20 points on the panel, see Figure 19, where the normal velocity of the panel is sequentially meas-

ured by a laser-scanning vibrometer (LSV). By identification of an extended model of the controlled plant which has additional velocity outputs, the controller is synthesized for global vibration reduction.

By means of Matlab/SIMULINK® and a dSPACE® rapid prototyping system the discrete state-space controllers were realized with a sampling frequency of 1 kHz. Calculation of radiated sound power bases on the vibration measurement with the LSV during operation of the controller and uses a frequency dependent 260 x 260 radiation resistance matrix [12]. The wind speed during tests was set to 55 m/s (= Mach 0.16). In Figure 20 and 21 the results of the experiments are shown. As expected, the vibration reduction of the global concept is best. At certain eigenfrequencies a reduction of factor 15 (= -11.8 dB) is realized. Thus, the inclusion of the scan point ve-

locities into the extended plant is able to realize global vibration reduction under TBL excitation. If the effort for generating the extended plant is taken into account, the local concept gains the best result. With only ten accelerometers the vibration reduction is close to this of the global concept.

The reduction of radiated sound power is shown in third-octave bands. As described above, sound power reduction can only be achieved at third-octave bands above 122 Hz, due to lack of controllability. In these thirds the global concept attains the best results with a maximum reduction of -6 dB(A) compared to the open-loop case.

4 From multibody simulations to acoustic analysis

Introduction

Besides aeroacoustic issues discussed so far, the noise generated at the wheel/rail-interface is a significant acoustic source as well [16]. It unfortunately contributes to the annoyance of railway noise particular in urban regions at low speed, see Figure 1.

As an additional aspect the work package to present in the following addresses an aim of the NGT project that concerns improvements of the virtual design process of railway vehicles. Modern engineering development flows rely on the capability of predicting properties of a specific product lay-out in an early stage and in a reliable and comprehensive manner.

Multi-body simulation in general and the multi-body code SIMPACK initially invented at the DLR in the 1990's in particular play an essential role in the initial design phase of railway vehicles in which conceptual issues are investigated. It is as well

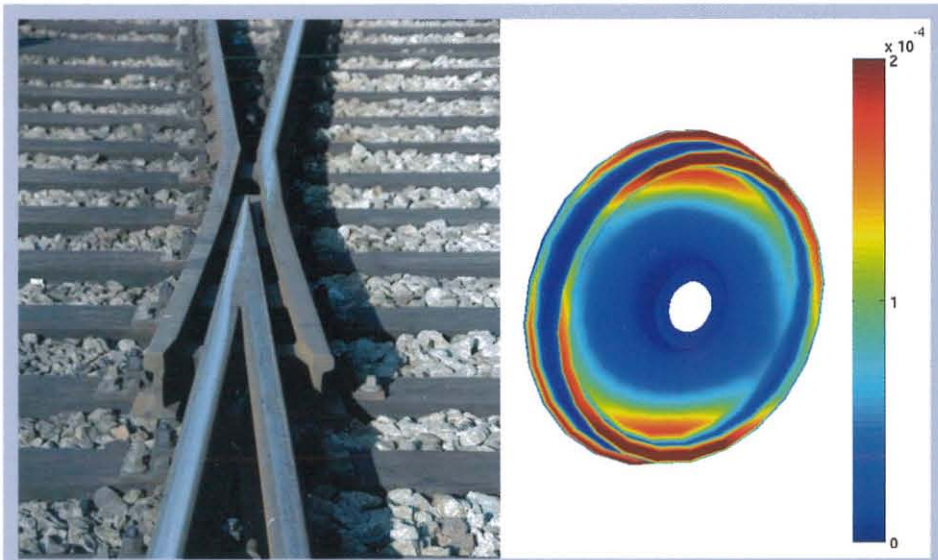


Figure 22: “Frog” and an example of the distribution of the structure borne sound intensity over the wheel surface (frame from a time simulation)

the state-of-the-art method in order to study and optimize the running dynamics and comfort of railway vehicles in details. However, acoustic issues could not be addressed so far by multi-body analysis. Firstly, this is due to the fact that the validity of the used multi-body models is usually restricted to the very low frequency range. Secondly, multi-body methodology is not prepared to evaluate acoustic measures in order to assess a railway vehicle under consideration. As already presented (cf. RTR Special – NGT: Running dynamics concept with mechatronic guidance) the first topic has been resolved in the course of the NGT project, since wheel, rail and contact models to be used in simulations in the frequency range up to 5 kHz have been introduced. This paper in particular addresses the second issue since the concept of an acoustic pre-processing tailored for multi-body analysis is proposed that is based on the evaluation of the sound power on the surface of vibrating elastic bodies.

Concept of acoustic post-processing

The usual way to represent flexible bodies in multi-body dynamics is a modal approach, i.e. the deformation field $\mathbf{u} = \mathbf{u}(\mathbf{x}, t)$ at a position \mathbf{x} of a flexible body is described

by a linear combination of spatial mode functions $\phi = \phi(\mathbf{x})$ with time-dependent modal amplitudes $q = q(t)$, i.e. $\mathbf{u} = \phi q$ [17]. As a consequence the normal velocity $v = v(\mathbf{x}_s, t)$ at the surface of the vibrating body under consideration may be evaluated as:

$$\mathbf{v}(\mathbf{x}_s, t) = \Phi_{\perp}(\mathbf{x}_s) \dot{\mathbf{q}}(t), \quad (1)$$

where $\dot{\mathbf{q}}(t)$ is the vector of generalized modal velocities and $\Phi_{\perp}(\mathbf{x}_s)$ the modal displacement normal to the surface at the position \mathbf{x}_s . These modal displacements may also be taken from a modal analysis of the underlying FE-model of the body.

As a consequence of (1), the squared value of the RMS velocity \bar{v}^2 over a time interval T can then be expressed as:

$$\bar{v}^2(\mathbf{x}_s, t) = \frac{1}{T} \int_0^T \dot{\mathbf{q}}^T \Phi_{\perp}^T \Phi_{\perp} \dot{\mathbf{q}} dt. \quad (2)$$

In addition the underlining operator is introduced now, which is to be applied to \mathbf{v} specifying the corresponding mean value over the surface S , i.e.

$$\underline{v}^2 = \frac{1}{S} \int_S v^2 ds = \dot{\mathbf{q}}^T \frac{1}{S} \int_S \Phi_{\perp}^T \Phi_{\perp} ds \dot{\mathbf{q}}. \quad (3)$$

The radiated sound power P for a vibrating body is then given by [6]:

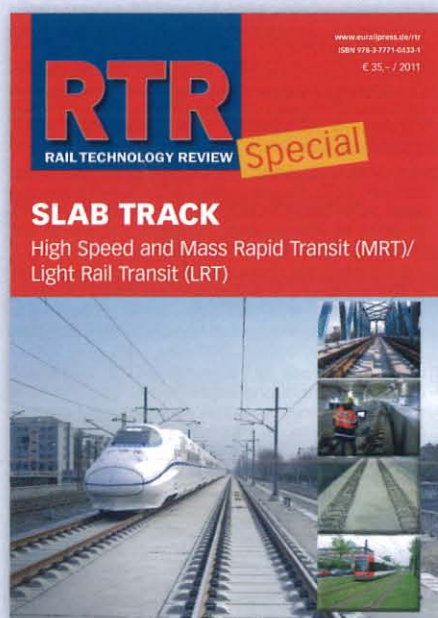
$$P = \sigma \rho c S \underline{v}^2, \quad (4)$$

where σ is the radiation efficiency, ρ the density of the air and c the corresponding sound velocity. The power is usually expressed as power level, i.e. as logarithm of the ratio of the power and a fixed reference quantity. The reader is referred to the corresponding norms for details (e.g. EN 21683 in Europe).

A central point is that the modal decomposition of the velocity in (1) leads to a separation of the problems in time and space. Consequently the integrations in time and spatial domain in (2) and (3) may be performed independently. In particular the computationally expensive surface integral in (3), now denoted by A , can be evaluated in advance and only once for a given flexible body:

$$\mathbf{A} = \int_S \Phi_{\perp}^T \Phi_{\perp} ds, \quad \underline{v}^2 = \dot{\mathbf{q}}^T \mathbf{A} \dot{\mathbf{q}}. \quad (5)$$

Once a multi-body simulation has been performed, the dynamics of the flexible body included in the model is known. It follows that the motion of every point on the surface of the vibrating bodies can be computed from the time histories of the modal coordinates, see (1). On this basis, the sound power on



Slab Track

– Second edition –

This second edition of the RTR Special Slab Track presents the **continuing development of systems and components together with exemplary applications** to you. The first edition in 2006 focussed on developments for high speed rail. In this edition the scope has been widened to Slab Track Systems in the fields of **Mass Rapid Transit (MRT) and Light Rail Transit (LRT)**.

The renowned experts **Dr. Edgar Darr and Dipl.-Ing. (FH) Werner Fiebig** give in an extensive survey a good introduction to this technically highly complex offering a comprehensive insight into slab track technology.

By now slab track technology is used throughout the world as **demonstrated by the examples** selected from Germany, Austria, India, China etc.

Technical Data: ISBN 978-3-7771-0433-1, 98 pages **Price:** EUR 35,- (incl. VAT, excl. postage)

Contact: DVV Media Group GmbH | Eurailpress, Phone: +49(0)40/2 37 14 - 440 • Fax: +49(0)40/2 37 14 - 450 • e-mail: book@dvvmedia.com

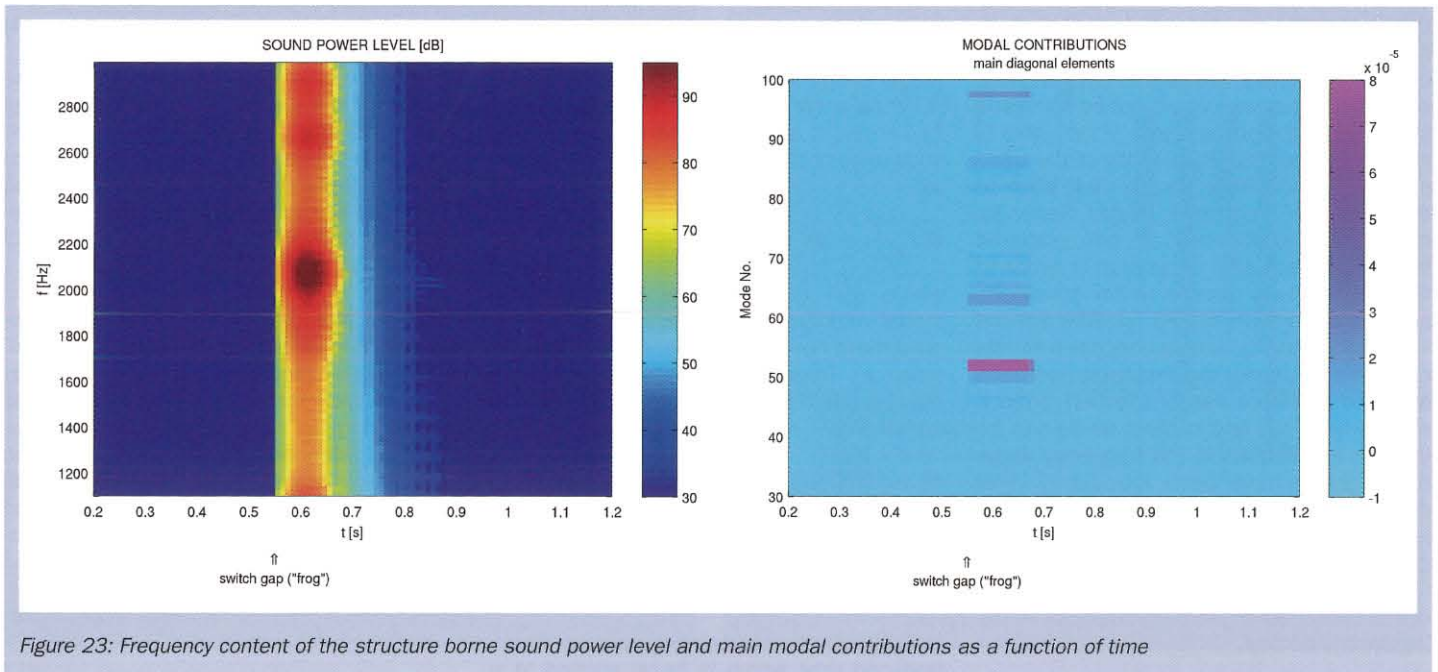


Figure 23: Frequency content of the structure borne sound power level and main modal contributions as a function of time

the body’s surface (structure borne sound) can be evaluated with very little additional computational effort, see [18] for a more detailed description of the acoustic post-processing.

Application example

The example scenario deals with a railway vehicle running through a switch. The vehicle is driving at 20 m/s and the leading wheel-set, the one modelled as flexible, encounters the rail gap in the centre part of a switch (so called “frog”, see Figure 22) at $t = 0.55$ s. The rail gap, modelled as a discontinuity in longitudinal direction, causes an impact of the wheel rolling over it; the induced vibration of the wheel-set originates impulsive noise.

The right hand side picture in Figure 22 presents an exemplary distribution of the structure borne sound intensity over the wheel surface at one specific point in time. It is not intended for a quantitative analysis but offers a valuable insight into the physical behaviour of the vibrating body.

Figure 23 shows the frequency content of the sound power level as a function of time on the left. A sliding time window of $T = 0.125$ s (denoted as “fast” in acoustic measurement engineering) has been used. It can be clearly seen that the noise due to the impact of the wheel over the rail gap is of very short duration and decays very rapidly. Note that the peak sound power level is very high (>90 dB). It must be stressed again that this value does not refer to a virtual receiver located somewhere near the wheel but to the power on the surface. Assuming a unitary radiation efficiency, $\sigma = 1$ in (4), as known to be the case for railway wheels above 1000 Hz, the decay due to the propagation should be considered to

eventually obtain, for example, the intensity at the standard railway measurement position at a distance of 7.5 m.

The sound power level in Figure 23 is dominated by a peak between 2000 and 2200 Hz. The proposed post-processing scheme also allows the modal contribution to be studied in order to determine those eigenmodes which are mainly responsible for this peak, namely the modes no. 51 and 52, see Figure 23 on the right hand side.

The main computational effort to simulate this application has been spent for the pre-processing, the FE modal analysis of the wheel-set which took less than one hour central processor unit-time on a modern 32 bit PC. The multi-body simulation and the post-processing did not require more than one minute cpu-time.

Finally it can be concluded that multi-body simulation is capable of carrying out acoustic assessment of railway vehicles. This will supplement tools currently used for this purpose. The presented methodology will be applied for further optimisation tasks in the course of the NGT project.

Sources

[1] Krüger, F. (Hrsg.): Schall-und Erschütterungsschutz im Schienenverkehr. expert-Verlag, Renningen, 2. Auflage. 2006
 [2] Talotte, C., Gautier, P-E., Thompson, D. J., Hanson, C.: Identification, modelling and reduction potential of railway noise sources: a critical survey, Journal of Sound and Vibration, Volume 267, Issue 3, Pages 447-468.
 [3] Lauterbach A., Grosche F. R.: Vorrichtung zur Ortung von Wellen mit mehreren Empfängern und einem Hohlspiegel Patent DE 10 2010 061 032.1-55
 [4] Lauterbach A., Ehrenfried K., Kröber S., Ahlefeldt T. and Loose, S.: Microphone array measurements on high-speed trains in wind tunnels, BeBeC-2010-01., 2010.

[5] Lauterbach A., Ehrenfried K. and Koop L.: Array measurements in wind tunnels with open test sections, BeBeC-2008-09, 2009.
 [6] Amiet R. K.: Correction of Open Jet Wind Tunnel Measurement for Shear Layer Refraction, 2nd AIAA Aeroacoustics Conference, Hampton, USA, AIAA-Paper 75-532, 1975
 [7] Lauterbach A., Ehrenfried K., Koop L. and Loose S.: Vorrichtung zur Bestimmung der akustischen Positionen von Mikrofonen im Raum Patent DE 10 2008 017 001.1-09
 [8] Lauterbach A., Ehrenfried K., Koop L. and Loose S.: Procedure for the accurate phase calibration of a microphone array, 15th AIAA/CEAS Aeroacoustics Conference, Miami, FL, USA, Number AIAA 2009-3122, 2009
 [9] Sijtsma P.: CLEAN based on spatial source coherence. AIAA Paper 2007-3436, 2007. 13th AIAA/CEAS Aeroacoustics Conference, Rome, Italy, 2007.
 [10] Ahlefeldt T., Lauterbach A. and Koop L.: Aeroacoustic Measurements of a scaled half model at high Reynoldsnumbers. 16th AIAA/CEAS Aeroacoustics Conference, Stockholm, Sweden, Number AIAA 2010-3748, 2010.
 [11] Lauterbach A., Ehrenfried K., Loose S. and Wagner C.: Scaling of Aeroacoustic Sources Measured on High-Speed Trains, 17th AIAA/CEAS Aeroacoustics Conference, Portland, OR, USA, Number AIAA 2011-2815, 2011
 [12] Algermissen, S., Misol, M., Unruh, O., Heintze, O. and Monner, H. P.: Robust control of turbulent boundary layer noise transmission through a stiffened panel. In Proc. of International Congress on Sound and Vibration, Cairo, Egypt, July 2010.
 [13] Algermissen, St., Rose, M., Keimer, R., Monner, H. P. and Breitbach, E.: Automated synthesis of robust controllers for smart-structure applications in parallel robots. In Proc. of AIAA/ASME/AHS Adaptive Structures Conference, Honolulu, USA, April 2007.
 [14] Heintze, O., Rose, M., Algermissen, St. and Misol, M.: Development and experimental application of a pre-design tool for active noise and vibration reduction systems. In Proceedings of ACTIVE 2009, Ottawa, Canada, 20-22 August 2009.
 [15] Katayama, T.: Subspace Methods for System Identification. Springer, 2005.
 [16] Thompson, D. J. and Jones, C.: A review of the modeling of wheel/rail noise generation. Journal of Sound and Vibration, 213(3):519–536, 2000.
 [17] Wallrapp, O.: Standardization of flexible body modeling in multibody system codes, Part 1: Definition of standard input data. Mech. Struct. Mach. 22(3), 283–304 (1994).
 [18] Heckmann, A., Kaiser, I. and Carrarini, A.: (2011) Bridging the Gap from Multibody Simulations to Acoustic Analysis. In: Noise and Vibration Mitigation for Rail Transportation Systems, 118. Springer-Verlag, Berlin, 2011.